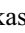


Molecular mechanical properties of short-sequence peptide enzyme mimics

Tsukasa Takahashi^a , Bao C. Vo Ngo^b, Leyang Xiao^b, Gaurav Arya^c and Michael J. Heller^{c,d*}

^aDepartment of Mechanical Engineering, University of California San Diego, 9500 Gilman Drive, La Jolla, CA 92093, USA;

^bDepartment of Chemical Engineering, University of California San Diego, 9500 Gilman Drive, La Jolla, CA 92093, USA;

^cDepartment of Nanoengineering, University of California San Diego, 9500 Gilman Drive, La Jolla, CA 92093, USA; ^dDepartment of Bioengineering, University of California San Diego, 9500 Gilman Drive, La Jolla, CA 92093, USA

Communicated by Ramaswamy H. Sarma

(Received 10 March 2015; accepted 7 April 2015)

While considerable attempts have been made to recreate the high turnover rates of enzymes using synthetic enzyme mimics, most have failed and only a few have produced minimal reaction rates that can barely be considered catalytic. One particular approach we have focused on is the use of short-sequence peptides that contain key catalytic groups in close proximity. In this study, we designed six different peptides and tested their ability to mimic the catalytic mechanism of the cysteine proteases. Acetylation and deacylation by Ellman's Reagent trapping experiments showed the importance of having phenylalanine groups surrounding the catalytic sites in order to provide greater proximity between the cysteine, histidine, and aspartate amino acid R-groups. We have also carried out all-atom molecular dynamics simulations to determine the distance between these catalytic groups and the overall mechanical flexibility of the peptides. We found strong correlations between the magnitude of fluctuations in the Cys-His distance, which determines the flexibility and interactions between the cysteine thiol and histidine imidazole groups, and the deacylation rate. We found that, in general, shorter Cys-His distance fluctuations led to a higher deacylation rate constant, implying that greater confinement of the two residues will allow a higher frequency of the acetyl exchange between the cysteine thiol and histidine imidazole R-groups. This may be the key to future design of peptide structures with molecular mechanical properties that lead to viable enzyme mimics.

Keywords: molecular dynamics simulations; enzyme mimics; peptide; molecular mechanics

1. Introduction

Nature has produced thousands of different enzymes through evolution that has resulted in highly efficient nanomachines that are unmatched in their catalytic properties. These nanomachines perform precise and specific catalysis with extremely high turnover rates for a wide variety of biochemical reactions. This phenomenon has resulted in many attempts to create purely artificial enzymes with enzyme-like activities (Bjerre, Rousseau, Marinescu, & Bols, 2008; Breslow, 2006; Raynal, Ballester, Vidal-Ferran, & van Leeuwen, 2014).

One of the most direct methods of mimicking an enzyme is to bring the key active site catalytic groups of an enzyme into close proximity with each other, in the same way they are found in natural enzymes (Jencks, 1963). The enzyme's ability to bind to substrates through the lock-and-key principle has produced legions of studies to create three-dimensional structures that combine both a binding site and a specific catalyst. The structures include peptides (Corey & Phillips, 1994; Rufo et al., 2014; Wharton, 1979), cyclodextrins (Houk, Leach, Kim, & Zhang, 2003; Rekharsky & Inoue, 1998),

metal-organic frameworks (Berg, 1993; Berg, 1995), nanoparticles and other synthetic nanostructures (Dong, Luo, & Liu, 2012; Kisailus, Truong, Amemiya, Weaver, & Morse, 2006; Kofoed & Reymond, 2005; Wei & Wang, 2013), and directed evolution of existing enzymes (Chica, Doucet, & Pelletier, 2005; Dalby, 2011; Gerlt & Babbitt, 2009; Kazlauskas & Lutz, 2009; Pleiss, 2012; Tobin, Gustafsson, & Huisman, 2000). However, despite these many efforts, the rate at which these molecules catalyze reactions is not nearly at the level of natural enzymatic turnover (Corey & Corey, 1996; Corey & Phillips, 1994; Korendovych & DeGrado, 2014).

In the cysteine protease, papain, there exists a catalytic triad that consists of Cys-25, His-159, and Asp-175 located in a precise three-dimensional space that allows minute mechanical movement to occur once a substrate is bound. The cysteine thiol anion acts as a nucleophile that attacks the amide or ester bond of the substrate while forming a covalent acyl-thiol intermediate. The histidine imidazole group provides general acid-base-assisted catalysis for proton abstraction and donation during the reaction. The aspartate carboxyl

*Corresponding author. Email: mheller@ucsd.edu

group plays a more secondary role in the overall catalytic reaction and we will be studying the effect of this group in our peptides (Beveridge, 1996; Drenth, Jansonius, Koekoek, Swen, & Wolthers, 1968; Harrison, Burton, & Hillier, 1997; Lake & Lowe, 1996; Tsukada & Blow, 1985).

We have recently shown a method in which short-sequence peptides containing the catalytic group of papain were used to mimic its hydrolysis reaction (Takahashi, Cheung, Butterweck, Schankweiler, & Heller, 2015). Nine different peptides were designed and tested for effectiveness of the Cys–His intermediate in short-sequence peptides. In particular, experiments were performed that proved that the back-attack reaction prevented the deacylation process of the acetyl group as shown in Figure 1. Once cleaved by the cysteine sulfhydryl group, the acetyl group exchange between the cysteine and histidine prevents the cysteine from proceeding with a new nucleophilic attack on the substrate. This back-attack mechanism was shown through NMR and Ellman's reagent trapping studies.

In this study, we show further acetylation and deacylation studies on a new set of peptides to get a better understanding of the important parameters to consider while designing peptides that mimic cysteine proteases. In addition to obtaining the experimental rates of acetylation and deacylation by Ellman's reagent trapping, we have carried out molecular dynamics simulations to determine the equilibrium structure and structural

fluctuations of each peptide at the experimental conditions. This structural analysis provides information on crucial physical parameters that control the back-attack and acetyl transfer mechanisms; specifically, the simulations allowed us to visualize and calculate the distances between Cys–His for each peptide structure and the overall end-to-end distance of each peptide. The Cys–His inter-residue distance is an obvious parameter to study, since the acetyl group exchange would only occur when the cysteine is brought close enough to attack the acetyl-imidazole bond. By analyzing the physical molecular distances, we are able to find a direct correlation between the computed Cys–His distance fluctuations and rate constants obtained in the actual experiments.

2. Experimental methods

2.1. Peptides

Six new peptides were designed and tested for their acetylation and deacylation rates. The sequences of these peptides are listed in Table 1 along with the previously studied peptides. Peptides 14, 16, and 18 vary by the addition of Phe and Gly–Phe between Lys–Cys, respectively. Peptides 15, 17, and 19 are the equivalents of Peptides 14, 16, and 18 with the addition of Phe–Asp at the C-terminus. These enzymes were designed to find the effects of chain length and the addition of aspartate next to the histidine on the N-terminus. Figure 2 shows Peptides 14 through 19 with color-coded cysteine and

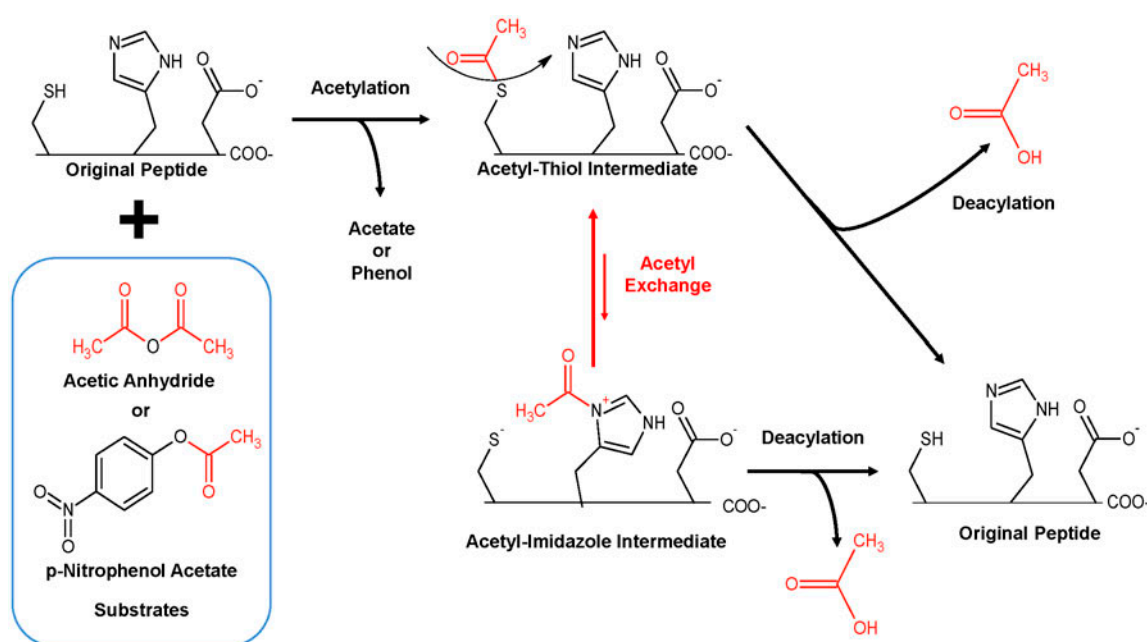


Figure 1. Scheme showing the peptide acetylation and deacylation process. The quick acetyl group exchange between the thiol and imidazole prevents turnover (Heller, Walder, & Klotz, 1977).

Table 1. List of controls and peptides with sequence.

Name	Compound/Sequence
Control 1	<i>p</i> -Nitrophenyl acetate (pNPA)
Control 2	Acetic anhydride (AA)
Control 3	<i>n</i> -Acetyl l-cysteine + <i>n</i> -acetyl l-histidine + <i>n</i> -acetyl l-lysine (ACAHAL)
Peptide 1	Ac-Gly-Gly-Ala-Ala-Cys-Ala-Ser-Ala-Asp
Peptide 2	Ac-Gly-Gly-Ala-Ala-Cys-Ala-His-Ala-Asp
Peptide 3	Ac-Arg-Gly-Ala-Ala-Cys-Ala-Ser-Ala-Asp
Peptide 4	Ac-Arg-Gly-Ala-Ala-Cys-Ala-His-Ala-Asp
Peptide 5	Ac-Arg-Gly-Ala-Phe-Cys-Phe-His-Ala-Asp
Peptide 6	Ac-Lys-Gly-Ala-Phe-Cys-Phe-His-Ala-Asp
Peptide 7	Ac-Arg-Asp-Phe-His-Phe-Cys-Ala-Gly-Asp
Peptide 8	Ac-Arg-Asp-Phe-Asn-Phe-Cys-Ala-Gly-Asp
Peptide 9	Ac-Arg-Gly-Gly-His-Phe-Cys-Gly-Pro-Gly-His-Gly-His-Gly-Asp
Peptide 14	Ac-Lys-Cys-Phe-His
Peptide 15	Ac-Lys-Cys-Phe-His-Phe-Asp
Peptide 16	Ac-Lys-Phe-Cys-Phe-His
Peptide 17	Ac-Lys-Phe-Cys-Phe-His-Phe-Asp
Peptide 18	Ac-Lys-Gly-Phe-Cys-Phe-His
Peptide 19	Ac-Lys-Gly-Phe-Cys-Phe-His-Phe-Asp

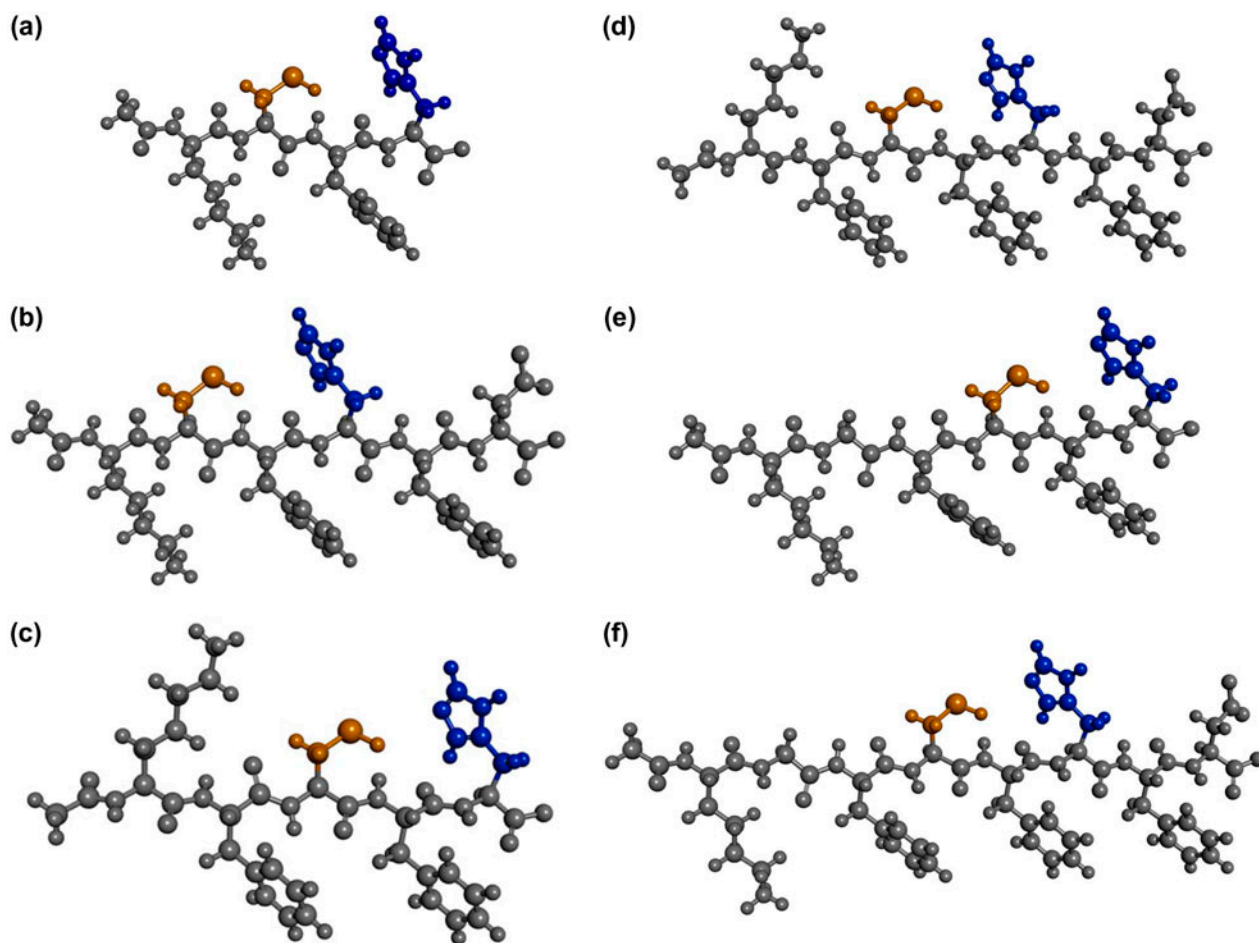


Figure 2. Peptides (a) 14, (b) 15, (c) 16, (d) 17 (e) 18, (f) 19 with cysteine and histidine labeled in orange and blue, respectively.

histidine. Peptides 2, 4, 5, 6, 7, and 9 were also used for the molecular dynamics simulations.

2.2. Acetylation

Peptides 14 through 19 were initially diluted to approximately 10 mM in DI water. The concentrations of the peptides were checked by measuring the total amount of cysteine using the Ellman's Reagent and comparing the 10 mM *n*-acetyl l-cysteine absorbance values at 412 nm. The substrate *p*-nitrophenyl acetate (pNPA) was diluted in ethanol, also to 10 mM. Each peptide was further diluted in 0.1 M tris-borate (TB) buffer, pH 8.5, and then the pNPA was added to start the reaction. The reaction was carried out at 20 °C for 30 min. The reaction concentration for both peptide and substrate was 100 μM in a final volume of 600 μL. The peptide reaction rates were determined along with Controls 1 and 2 – each substrate for acetylation and deacylation alone; and Control 3 – 100 μM of *n*-acetyl l-cysteine (AC), *n*-acetyl l-histidine (AH), and *n*-acetyl l-lysine (AL). The absorbance of the cleaved *p*-nitrophenol was measured at 400 nm with a Perkin Elmer UV-vis Lambda 800 during the 20-min reaction time. The second-order rate constants for the acetylation process were determined from the initial rates according to the equation:

$$k_a = \frac{\text{initial rate} - \text{spontaneous rate}}{[\text{catalyst}][\text{substrate}]}$$

where the spontaneous rate is the hydrolysis rate of pNPA.

For Peptides 18 and 19, additional acetylation experiments were performed at five pH values in 0.1× TB buffer and 4× substrate concentrations of 2 mM. This test was performed in order to see the effect of the imidazole changing the pK_a of the neighboring cysteine thiol. The cysteine thiol ($pK_a = 8.14$) is normally 10% deprotonated at pH 7.2; 25% at pH 7.74; 50% at pH 8.14; 75% at pH 8.67, and 90% at pH 9.13.

2.3. Deacylation & Ellman's Reagent trapping

Initially, Peptides 14 through 19 were acetylated with a 15-fold excess of acetic anhydride (AA) injected as a 10% by volume solution in acetonitrile. The acetylation of the imidazole and the thiol groups of the peptides was observed for 20 min at 270 nm and 235 nm, respectively, to ensure the completion of the reaction. Subsequently, deacylation by trapping was examined by adding Ellman's reagent (5,5'-dithiobis-(2-nitrobenzoic acid)) at four times the concentration of the peptides and the controls. Ellman's reagent irreversibly alkylates the free thiol anion when the acetyl group transfers from the thiol to the imidazole. This trapping reaction prevents

back-attack by the thiol group, allowing the acetyl-imidazole group to deacylate. The deacylation of the acetyl-imidazole correlates with increase in absorbance of the cleaved Ellman's reagent (2-nitro-5-thiobenzoate) at 412 nm. A first-order rate constant for the deacylation process was determined with the initial rate according to the equation:

$$k_d = \frac{\text{initial rate}}{[\text{catalyst}]}$$

2.4. Molecular Dynamics (MD) simulations

To investigate the structural dynamics of each of the peptides, we performed implicit-solvent MD simulations at the experimental conditions. The molecular interactions were treated using the CHARMM27 force field (MacKerell, Banavali, & Foloppe, 2000) and the simulations were performed using the NAMD package (Phillips et al., 2005). The effects of the solvent were treated implicitly using the Generalized Born model (Onufriev, Bashford, & Case, 2004), where the dielectric constants of the protein and solvent are 1 and 78.5, respectively. In addition, the monovalent ion concentration is set at 0.008 M along with a temperature of 293 K to reflect the 0.1× TB condition at room temperature employed in the experiments.

Five independent MD trajectories, each 60 ns long with a time step of 2 fs, were performed for each peptide. Atomic structures of the peptides for starting the simulations were created in Accelrys Discovery Studio 3.5 (Discovery Studio Modeling Environment, 3.5; Pdb Molecule Builder, 2013) and then energy-minimized with 100 steps of conjugate gradient in NAMD. The target temperature of 293 K was maintained using a Langevin thermostat with a damping coefficient of 1 ps⁻¹. To avoid instability, the bonds connecting hydrogen to other atoms were constrained using the SHAKE algorithm. We employed cut-off and switch distances for nonbonding interactions of 14.0 Å and 13.0 Å, respectively. The conformations were saved every 250 steps (5×10^{-4} ns) while the energies are saved every 100 steps or 2×10^{-4} ns. We used the last 50 ns of the MD trajectories (production runs) to analyze two types of intermolecular distances: 1) the interresidue distances as the peptides undergo conformational dynamics, and 2) the end-to-end distance to measure the overall peptide conformation.

3. Results

3.1. Acetylation

Acetylation rates of Peptides 14 through 19 are shown in Figure 3. Although the acetylation rates of the peptides

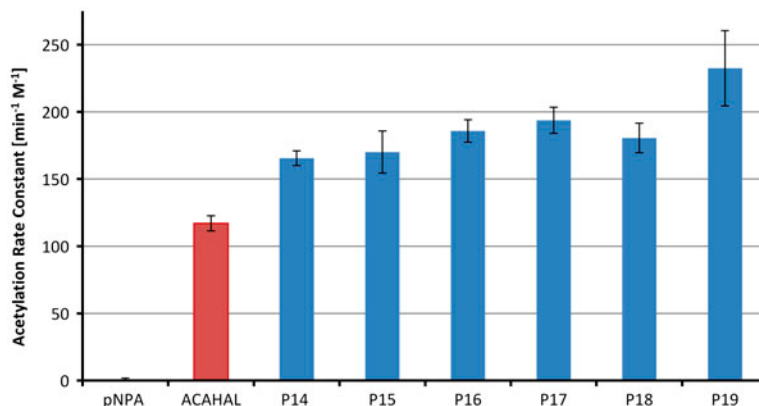


Figure 3. Acetylation rate constants of Peptide 14 through 19 and controls.

were slightly higher than the lone amino acid control (ACAHAL), we did not see a significant increase. While unexceptional, these increases are related to the increase in nucleophilic attack by the thiol anion. The presence of histidine on the same peptide backbone allows the thiol anion to become more nucleophilic. The back-attack by the thiol is present, and this prevents the effective turnover that we hope to see.

Peptides 18 and 19 were further studied to see the effect of lowering of the pH and the results are shown in Figure 4. As the pH is lowered, it was expected that that the thiol would become less reactive due to protonation. However, on the peptides, the thiol pK_a is lowered by its close proximity to histidine, unlike the controls that have individual amino acids at longer range. This effect was previously seen in Peptide 6 and was expected in Peptides 18 and 19 as well. As the pH is lowered below the thiol pK_a (pH 8.15), the rate ratio between P18/P19 and ACAHAL increases. At pH 7.20, the deacylation rate ratio of Peptide 18/ACAHAL is 1.80 and Peptide

19/ACHAL is 1.40. Although the lowering of the thiol pK_a was observed for the peptides, it is interesting to note that Peptide 19, which contains the extra Phe-Asp at the N-terminus, had no effect on further changing the pK_a of the cysteine.

3.2. Deacylation

Deacylation rate constants of Peptides 14 through 19 are shown in Figure 5. Although all peptides achieved higher deacylation rates, they are very similar, excluding Peptide 15. These rates are comparable to the previously studied Peptides 2 through 9 and further prove the importance of having the cysteine thiol surrounded by phenylalanines. The effect of steric hindrance created by the bulky phenylalanine residues is present even with a length of four amino acids. Although we had hoped to see a greater effect of the Phe-Asp added at the N-terminus, there was no significant difference seen in the deacylation rates.

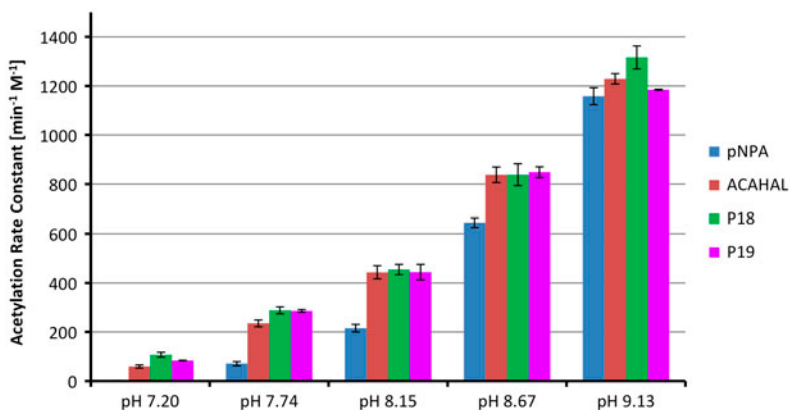


Figure 4. Acetylation rate constants of Peptides 18, 19, and controls at variable pH 7.20 (10% S-), pH 7.74 (25% S-), pH 8.15 (50% S-), pH 8.67 (75% S-), and pH 9.13 (90% S-).

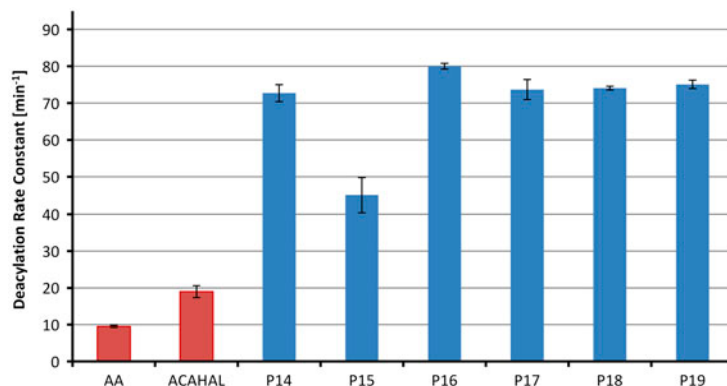


Figure 5. Deacylation rate constants of Peptide 14 through 19 and controls.

3.3. MD analysis

Simulations were performed on the previously studied Peptides 2 through 9 as well as the new Peptides 14 through 19. Each 60 ns-long simulation yielded 120,000

distance values, taken between the lone nitrogen atom of histidine and the sulfur atom of cysteine for the Cys–His interresidue distances, and the carbon atom of the C-terminus and the nitrogen atom of the N-terminus for

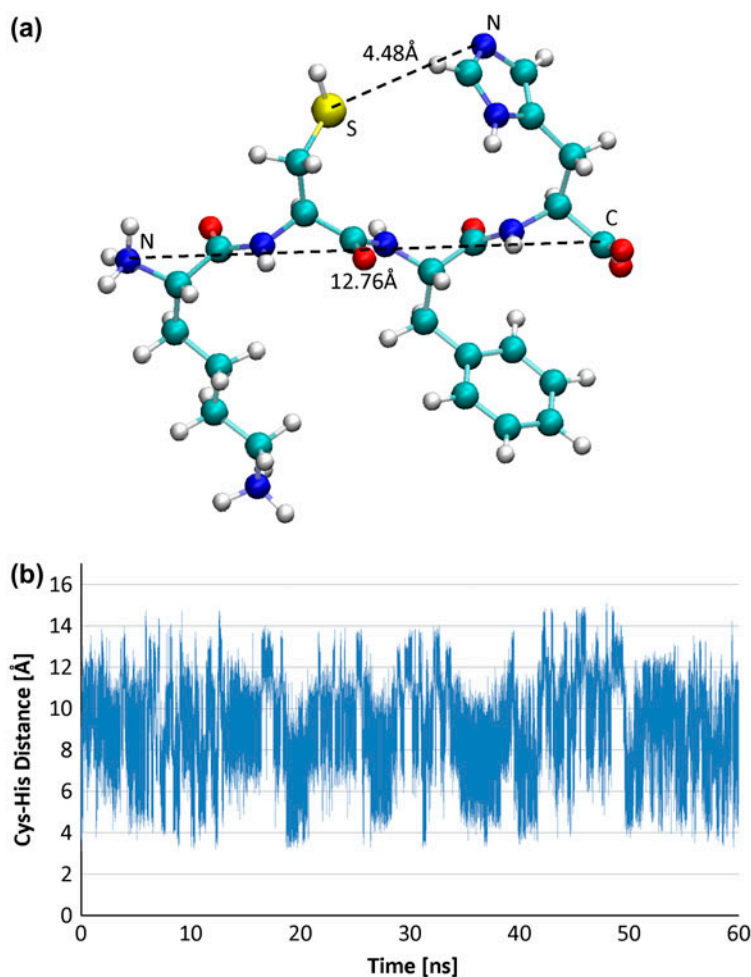


Figure 6. (a) Representative conformation of Peptide 14 with labelled Cys-His interresidue distance as 4.48 Å and end-to-end distance as 12.76 Å. (b) Plot of Cys-His distance vs. time obtained from one of the simulations of Peptide 14. The image of the peptide was generated using the program VMD (Humphrey, Dalke, & Schulten, 1996).

the end-to-end distances. The distance data were imported into Excel where they were plotted against time frames. Figure 6a presents a representative conformation of Peptide 14 obtained during one of the simulations, with labeled Cys-His and end-to-end distances. Figure 6b shows a plot of the Cys-His distance vs. time over a 60 ns simulation run. Note that we performed five such simulations per peptide.

The two main differences between our model peptides and those studied experimentally are (1) the missing acetyl-thiol or acetyl-imidazole group and (2) the acetyl terminated C-terminus; this is because the force field parameters for the acetyl-thiol or acetyl-imidazole groups and acetylated C-terminus amino acids are currently not available or well established. The simplified model may provide slightly unrealistic results since the interaction on which we are focusing occurs during the acetyl exchange. However, the general Cys-His measurements should give us useful insight as to how the neighboring residues affect the interresidue distance. The nonacetylated C-terminus may have a slight effect on the flexibility of the entire peptide, but we should see minimal difference for our final results.

The Cys-His interresidue average distances were plotted for all peptides with the deacylation rate constants to check for correlation. We hypothesized that the smaller the interresidue distances of a peptide, the larger its corresponding deacylation constant due to the frequency of interaction between the amino acids. However, the plot had a weak negative correlation with an R^2 value of 0.0025. Dividing the peptides between 2 through 9 and 14 through 19, the correlation was still weak at R^2 values of 0.20 and 0.21, respectively. The average distances for Peptides 14 through 19 increased from 9.24 to 9.88 Å with the exception of Peptide 15 with 9.14 Å.

Investigating further, we noticed a correlation between the Cys-His distance deviation, which shows the strong variability in the simulations (see Figure 6b), and the deacylation rate constant. As plotted in Figure 7, there is a strong correlation between the distance deviation and deacylation rate constants for Peptides 2, 4, 5, and 6. These peptides are very closely related in terms of peptide length, and their amino acid sequence varies only in the C-terminus amino acid (Gly, Arg, and Lys) and the amino acids surrounding the cysteine (Ala-Cys-Ala or Phe-Cys-Phe). Peptides 2 and 4 showed higher distance deviation than Peptides 5 and 6. This shows that the cysteine surrounded by alanine allows larger variability in intermolecular distances between the histidine and cysteine, which is unfavorable for the acetyl exchange. From this particular set of results, it may be concluded that smaller deviations in the Cys-His distance allow more interactions between the two residues, likely due to the increased confinement in the structure stemming from the larger residues.

From the same series of peptides, Peptide 9, which contains three extra residues and two more histidines, achieved a much lower Cys-His distance deviation at 1.20 Å, but only reached a deacylation rate slightly higher than Peptide 5. Also, Peptide 7, which has the reverse order of cysteine and histidine, and also a low distance deviation at 1.38 Å, had a poor correlation to its low deacylation rate compared to Peptides 2, 4, 5, and 6. This shows that this method of correlation needs to be used with caution and may work best when peptides with very similar sequences are compared.

The Cys-His distance deviation and rate constants of Peptides 14 through 19 are plotted in Figure 8. The R^2 value for this correlation is 0.53, which shows only moderate correlation between the distance and the rates. However, it is notable that Peptide 15, which had the

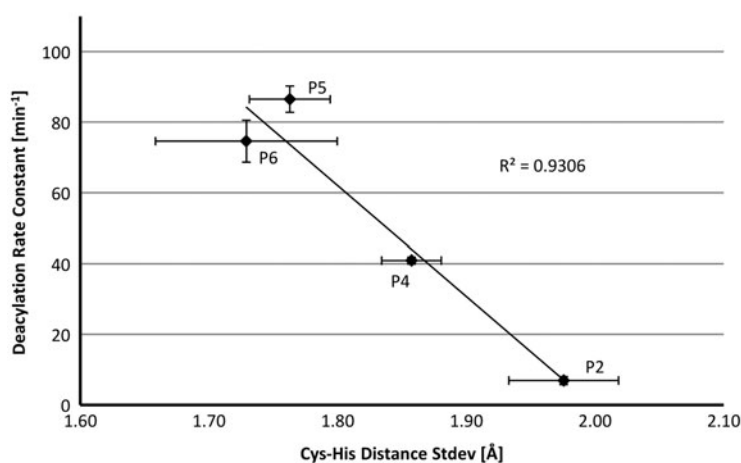


Figure 7. Cys-His distance deviation vs. deacylation rate constant for Peptides 2, 4, 5, and 6.

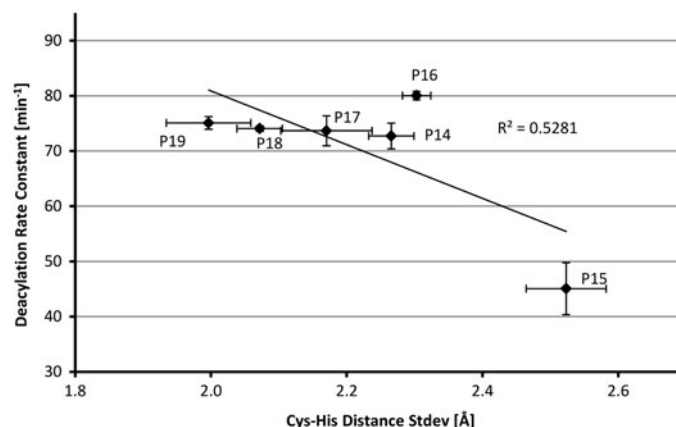


Figure 8. Cys-His distance deviation vs. deacylation rate constant for Peptides 14 through 19.

greatest distance deviation at 2.53 Å, achieved roughly half the deacylation rate constant as other peptides. This may indicate an existence of a threshold distance deviation that is necessary to achieve a certain rate constant. If the distance varies too much, this is an indication that

there are fewer chances for the thiol anion to attack the acetyl-imidazole.

Figure 9 shows the end-to-end distances of Peptides 14 through 19 in relation to the Cys-His distance deviation. It is noted that longer peptides have a longer

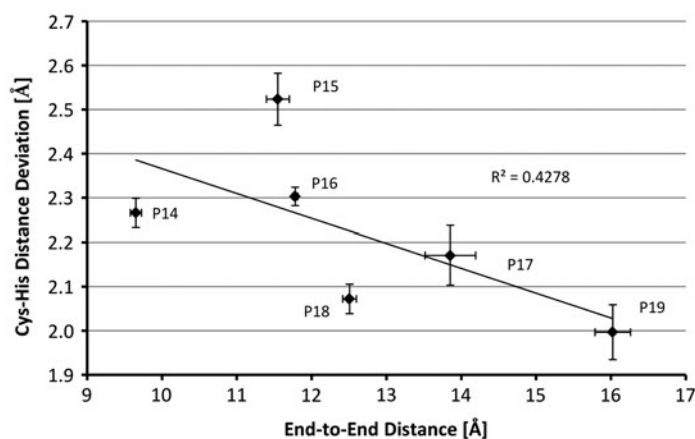


Figure 9. End-to-end distance vs. Cys-His distance deviation of Peptides 14 through 19.

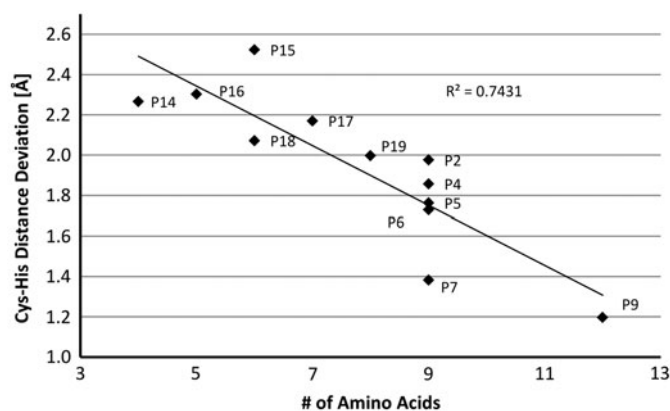


Figure 10. Number of amino acids vs. Cys-His distance deviation for all peptides.

Table 2. Length of the peptides studied here along with their measured deacylation rate constant, Cys–His distance, and end-to-end distance.

	# of amino acid	Deacylation rate constant (min^{-1})	Cys–His distance		End-to-end distance	
			Average (Å)	Deviation (Å)	Average (Å)	Deviation (Å)
P2	9	6.9	9.92	1.98	15.39	3.90
P4	9	40.9	9.89	1.86	12.88	4.00
P5	9	86.5	10.18	1.76	13.23	4.45
P6	9	74.6	9.94	1.73	15.83	3.82
P7	9	25.5	10.27	1.38	14.86	3.52
P9	12	88.4	10.41	1.20	14.30	6.26
P14	4	72.7	9.24	2.27	9.65	2.02
P15	6	45.1	9.14	2.52	11.55	3.52
P16	5	80.0	9.32	2.30	11.78	2.23
P17	7	73.7	9.32	2.17	13.85	4.44
P18	6	74.1	9.83	2.07	12.51	2.90
P19	8	75.1	9.88	2.00	16.02	5.01

end-to-end distance, which contributes to a shorter Cys–His distance deviation. Although longer molecules are generally more flexible, the flexibility also depends on the residue size, with larger residues lowering the flexibility of the peptide chain due to larger rotational barriers (Huang & Nau, 2003; Janin & Sternberg, 2013; Mierke, Kurz, & Kessler, 1994; Pornsuwan, Bird, Schafmeister, & Saxena, 2006). A simple plot of number of amino acids in the peptide vs. the Cys–His distance deviation is shown in Figure 10. This correlation achieved a high R^2 value of 0.74. Although it is possible to simply increase the length of the peptide, Peptide 9, which has three more residues than Peptide 5, only achieved a marginal rate increase. It is difficult to directly compare these two peptides since Peptide 9 also contains two extra histidine molecules that could react with the acetyl-thiol intermediate at any time. Further MD simulations with variations of peptide amino acid chain length and number of histidine molecules will be necessary to see the effect of the extra histidine molecules.

Table 2 provides the compiled distance results and deacylation rate constants for each peptide.

4. Discussion

4.1. Cys–His distance deviation and acetyl transfer rate

Our acetylation and deacylation results, the importance of surrounding the cysteine group with bulky amino acids can be emphasized again. The Cys–His and end-to-end distances confirm that the acetyl transfer occurs at greater rates for peptides with a more confined geometry. There are several ways in which this can be achieved. The first is to implement a rigid structure intrinsically through the design process of these peptides. Like natural enzymes, a more precise interresidue geometry is

necessary in order to let the acetyl transfer occur. Longer chains have proven that they can produce a more rigid Cys–His structure. Further incorporation of known structures such as protein folds and helices may be helpful. Another method is to confine these peptides within known boundaries and configurations. This can be achieved by attaching one or both ends of the peptide to a structure such as a metallic surface or to nanoparticles. By anchoring the terminus of the peptide, the flexibility of the peptide will be greatly reduced, allowing a more controlled interaction between the amino acids. In addition to controlling one end of the peptide, attaching peptides on surfaces allows the application of other external forces (electric field, fluidic, or acoustic) that can be used to assist the mechanical activity of the peptides. Our present hypothesis is that the application of a directional oscillating or pulsing DC or AC electric field may ultimately provide the mechanism for preventing back attack and producing turnover. Chen et al. have shown a sensor mechanism that measures for phosphorylated and non-phosphorylated peptides attached to a metallic surface by applying a DC voltage. The phosphorylated peptides collapse while the electric field is applied, but the non-phosphorylated peptides remain insensitive to the field, allowing for kinase reactions to occur (Chen et al., 2012). Application of any form of external force introduces a variety of parameters that can be adjusted. With the help of experimental and modeling data, these parameters could be tuned to control the peptide conformations and optimization becomes possible for many reactions. Further utilization nonpeptide based catalysts, such as metal ions, allows for many possible forms of catalytic reactions.

Although we have focused on the rate at which the acetyl group transfers between the cysteine and histidine, our attention should also be on controlling the inter-residue distance so that the deacylation process can occur

from the acetyl-histidine as shown in Figure 1. To truly achieve this step, the interresidue distance must be increased to prevent the thiol back-attack from occurring. This is the opposite approach to our current studies, which focus on bringing the two residues closer to achieve higher interaction. The level of control that is required to adjust these intermolecular distances at will is a challenging task and will require a smart design that allows peptide conformation to recognize and react to a certain binding pattern.

4.2. Relation to intrinsically disordered proteins (IDP)

Although the crystal structures of proteins have been studied for decades, there has been an increased interest in proteins that contain disordered peptide chains during the binding process or at the transition state of a reaction. These proteins are known as IDP and are characterized by their lack of structure for some or all of their peptide chains, which assist reactions by creating different binding/inhibiting structures (Dunker et al., 2001; Wright & Dyson, 2015). While many focus on finding the crystal structure of the proteins, the known structures do not tell the full story of which protein produced the product. Specifically, there are protein complexes that start with an ordered state and transition through a molten globular state such as fd phage and histone octamer. There are also proteins such as histone H4 in nucleosomes (Yang & Arya, 2011) and trypsinogen that undergo disorder-to-order transitions to mediate protein-protein interactions or to become fully active enzymes (trypsin) (Dunker et al., 2001).

Our peptides are similar in concept to some of these IDPs; in order to achieve substrate binding and effective acetyl transfer, the peptides require low disorder. However, once the transition has taken place from acetyl-thiol to acetyl-imidazole, greater disorder is required to achieve deacylation. A possible solution for this process may be an additional charge-changing reaction that utilizes the rest of the inactive amino acids on the peptide chain, similar to the Asp-175 present in papain. Studies of these proteins may help design a new set of proteins and enzymes that can produce catalysis through its controlled order/disorder.

4.3. MD simulations

Our simulation studies have been useful for investigating the dynamics of these peptides in a controlled environment. Although, these simulation results must be taken with caution because the parameters do not represent the experimental conditions exactly, useful qualitative insights can still be made. The main difference between our simulation models of peptides and the experimental peptides is the missing acetyl group on the thiol or the imidazole to

represent the acetyl group transfer. In future studies, we plan to rigorously derive molecular-mechanics forcefield parameters for the acetyl-thiol and acetyl-imidazole intermediates and use these in place of thiol and imidazole groups to investigate inter-residue distances in an environment that is more reflective of the experimental peptides.

In papain, the Cys–His interresidue distance is roughly 6 Å when measured from the PDB crystal structure (Drenth et al., 1968). Although we could use this distance as a reference point to build our peptides, it should be kept in mind that the papain macromolecular structure produces precise movements during catalysis that we do not completely understand. From our results, it may be suggested that Asp-175 has little effect on the actual catalytic triad, which leads us to believe that the actual papain mechanism is dominated by the cysteine–thiol and histidine–imidazole interactions.

5. Conclusion

In conclusion, six new catalytic peptides were designed to investigate their reaction rates. The acetylation and deacylation rate constants showed consistency with previously studied peptides and confirmed the importance of steric hindrance created by phenylalanine. Furthermore, MD simulations showed signs of higher acetyl transfer rates being related to the overall peptide length and the Cys–His interresidue distance deviation. Future peptides will be designed using modeling first to confirm a lower Cys–His distance deviation. Although our studies have focused on the acetyl transfer rate, it is important that future experimental designs be directed at achieving secondary conformational changes that lead to true catalytic turnover, i.e. deacylation without Ellman's Reagent trapping. Thus, future work will focus on both structural improvements and the application of external electric fields to produce desired nanomechanical properties for achieving turnover.

Abbreviations

NMR	nuclear magnetic resonance
NAMD	not another molecular dynamics
VMD	visual molecular dynamics
TB	tris-borate

Author contributions

The manuscript was written through contributions of all authors. All authors have given approval to the final version of the manuscript.

Acknowledgment

Authors would like to thank Dr Jennifer Wright for her help in preparing the manuscript and Amy Pan for her assistance in analyzing the NAMD data.

Disclosure statement

No potential conflict of interest was reported by the authors.

ORCID

Tsukasa Takahashi  <http://orcid.org/0000-0002-6395-9193>

References

- Berg, J. M. (1993). Zinc-finger proteins. *Current Opinion in Structural Biology*, 3, 11–16.
- Berg, J. M. (1995). Zinc finger domains: From predictions to design. *Accounts of Chemical Research*, 28, 14–19.
- Beveridge, A. J. (1996). A theoretical study of the active sites of papain and s195c rat trypsin: Implications for the low reactivity of mutant serine proteinases. *Protein Science*, 5, 1355–1365.
- Bjerre, J., Rousseau, C., Marinescu, L., & Bols, M. (2008). Artificial enzymes, “chemzymes”: Current state and perspectives. *Applied Microbiology and Biotechnology*, 81(1), 1–11.
- Breslow, R. (2006). *Artificial enzymes* (pp. 1–35). New York, NY: Wiley-VCH Verlag GmbH & Co. KGaA.
- Chen, Y., Cruz-Chu, E. R., Woodard, J. C., Gartia, M. R., Schulten, K., & Liu, L. (2012). Electrically induced conformational change of peptides on metallic nanosurfaces. *ACS Nano*, 6, 8847–8856.
- Chica, R. A., Doucet, N., & Pelletier, J. N. (2005). Semi-rational approaches to engineering enzyme activity: Combining the benefits of directed evolution and rational design. *Current Opinion in Biotechnology*, 16, 378–384.
- Corey, D. R., & Phillips, M. A. (1994). Cyclic peptides as proteases: A reevaluation. *Proceedings of the National Academy of Sciences*, 91, 4106–4109.
- Corey, M. J., & Corey, E. (1996). On the failure of de novo-designed peptides as biocatalysts. *Proceedings of the National Academy of Sciences*, 93, 11428–11434.
- Dalby, P. A. (2011). Strategy and success for the directed evolution of enzymes. *Current Opinion in Structural Biology*, 21, 473–480.
- Discovery Studio Modeling Environment, 3.5; Pdb Molecule Builder. (2013). San Diego, CA: Accelrys Software.
- Dong, Z., Luo, Q., & Liu, J. (2012). Artificial enzymes based on supramolecular scaffolds. *Chemical Society Reviews*, 41, 7890–7908.
- Drenth, J., Jansonius, J. N., Koekoek, R., Swen, H. M., & Wolthers, B. G. (1968). Structure of papain. *Nature*, 218, 929–932.
- Dunker, A. K., Lawson, J. D., Brown, C. J., Williams, R. M., Romero, P., Oh, J. S., ... Obradovic, Z. (2001). Intrinsically disordered protein. *Journal of Molecular Graphics and Modelling*, 19, 26–59.
- Gerlt, J. A., & Babbitt, P. C. (2009). Enzyme (re)design: Lessons from natural evolution and computation. *Current Opinion in Chemical Biology*, 13, 10–18.
- Harrison, M. J., Burton, N. A., & Hillier, I. H. (1997). Catalytic mechanism of the enzyme papain: Predictions with a hybrid quantum mechanical/molecular mechanical potential. *Journal of the American Chemical Society*, 119, 12285–12291.
- Heller, M. J., Walder, J. A., & Klotz, I. M. (1977). Intramolecular catalysis of acylation and deacylation in peptides containing cysteine and histidine. *Journal of the American Chemical Society*, 99, 2780–2785.
- Houk, K. N., Leach, A. G., Kim, S. P., & Zhang, X. (2003). Binding affinities of host–guest, protein–ligand, and protein–transition-state complexes. *Angewandte Chemie International Edition*, 42, 4872–4897.
- Huang, F., & Nau, W. M. (2003). A conformational flexibility scale for amino acids in peptides. *Angewandte Chemie International Edition*, 42, 2269–2272.
- Humphrey, W., Dalke, A., & Schulten, K. (1996). Vmd: Visual molecular dynamics. *Journal of Molecular Graphics*, 14, 33–38.
- Janin, J., & Sternberg, M. J. E. (2013). Protein flexibility, not disorder, is intrinsic to molecular recognition. *F1000 Biology Reports*, 5, 2.
- Jencks, W. P. (1963). Mechanism of enzyme action. *Annual Review of Biochemistry*, 32, 639.
- Kazlauskas, R., & Lutz, S. (2009). Engineering enzymes by ‘intelligent’ design. *Current Opinion in Chemical Biology*, 13(1), 1–2.
- Kisailus, D., Truong, Q., Amemiya, Y., Weaver, J. C., & Morse, D. E. (2006). Self-assembled bifunctional surface mimics an enzymatic and templating protein for the synthesis of a metal oxide semiconductor. *Proceedings of the National Academy of Sciences*, 103, 5652–5657.
- Kofoed, J., & Reymond, J. L. (2005). Dendrimers as artificial enzymes. *Current Opinion in Chemical Biology*, 9, 656–664.
- Korendovych, I. V., & DeGrado, W. F. (2014). Catalytic efficiency of designed catalytic proteins. *Current Opinion in Structural Biology*, 27, 113–121.
- Lake, A. W., & Lowe, G. (1966). The kinetics of papain- and ficin-catalysed hydrolyses in the presence of alcohols. *Biochemical Journal*, 101, 402–410.
- MacKerell, A. D., Banavali, N., & Foloppe, N. (2000). Development and current status of the charmm force field for nucleic acids. *Biopolymers*, 56, 257–265.
- Mierke, D. F., Kurz, M., & Kessler, H. (1994). Peptide flexibility and calculations of an ensemble of molecules. *Journal of the American Chemical Society*, 116, 1042–1049.
- Onufriev, A., Bashford, D., & Case, D. A. (2004). Exploring protein native states and large-scale conformational changes with a modified generalized born model. *Proteins: Structure, Function, and Bioinformatics*, 55, 383–394.
- Phillips, J. C., Braun, R., Wang, W., Gumbart, J., Tajkhorshid, E., Villa, E., ... Schulten, K. (2005). Scalable molecular dynamics with namd. *Journal of Computational Chemistry*, 26, 1781–1802.
- Pleiss, J. (2012). Rational design of enzymes. In K. Drauz, H. Gröger, & O. May (Eds.), *Enzyme catalysis in organic synthesis* (pp. 89–117). Stuttgart: Wiley-VCH Verlag GmbH & Co. KGaA.
- Pornsuwan, S., Bird, G., Schafmeister, C. E., & Saxena, S. (2006). Flexibility and lengths of bis-peptide nanostructures by electron spin resonance. *Journal of the American Chemical Society*, 128, 3876–3877.
- Raynal, M., Ballester, P., Vidal-Ferran, A., & van Leeuwen, P. W. N. M. (2014). Supramolecular catalysis. Part 2: Artificial enzyme mimics. *Chemical Society Reviews*, 43, 1734–1787.
- Rekharsky, M. V., & Inoue, Y. (1998). Complexation thermodynamics of cyclodextrins. *Chemical Reviews*, 98, 1875–1918.
- Rufo, C. M., Moroz, Y. S., Moroz, O. V., Stöhr, J., Smith, T. A., Hu, X., ... Korendovych, I. V. (2014). Short peptides self-assemble to produce catalytic amyloids. *Nature Chemistry*, 6, 303–309.
- Takahashi, T., Cheung, M., Butterweck, T., Schankweiler, S., & Heller, M. J. (2015). Quest for a turnover mechanism in peptide-based enzyme mimics. *Catalysis Communications*, 59, 206–210.

- Tobin, M. B., Gustafsson, C., & Huisman, G. W. (2000). Directed evolution: The 'rational' basis for 'irrational' design. *Current Opinion in Structural Biology*, *10*, 421–427.
- Tsukada, H., & Blow, D. M. (1985). Structure of alpha-chymotrypsin refined at 1.68 Å resolution. *Journal of Molecular Biology*, *184*, 703–711.
- Wei, H., & Wang, E. (2013). Nanomaterials with enzyme-like characteristics (Nanozymes): Next-generation artificial enzymes. *Chemical Society Reviews*, *42*, 6060–6093.
- Wharton, C. W. (1979). Synthetic polymers as models for enzyme catalysis—a review. *International Journal of Biological Macromolecules*, *1*, 3–16.
- Wright, P. E., & Dyson, H. J. (2015). Intrinsically disordered proteins in cellular signalling and regulation. *Nature Reviews Molecular Cell Biology*, *16*, 18–29.
- Yang, D., & Arya, G. (2011). Structure and binding of the H4 histone tail and the effects of lysine 16 acetylation. *Physical Chemistry Chemical Physics*, *13*, 2911–2921.